Polymer 177 (2019) 84–90

Contents lists available at ScienceDirect

Polymer

journal homepage: www.elsevier.com/locate/polymer

Construction of master yield stress curves for polycarbonate: A coarse-grained molecular dynamics study

Atsushi Kubo, Jan-Michael Albina*, Yoshitaka Umeno

Institute of Industrial Science, The University of Tokyo, 4-6-1 Komaba Meguro-ku, Tokyo 153-8505, Japan

HIGHLIGHTS

- A coarse-grained model is developed to study deformations in polycarbonate.
- Various deformation modes are investigated.
- The critical yield stress is evaluated at different strain rates and temperatures.
- Multi-temperature and multi-loading master yield stress curves are built.

ARTICLE INFO

Keywords:
Polycarbonate
Molecular dynamics
Coarse-grained particle
Deformations
Multiaxial loading
Yield stress
Strain rate

ABSTRACT

A coarse-grained particle model was developed for the simulation of deformations in polycarbonate. Coarse-grained molecular dynamics simulations of uniaxial and multiaxial deformations are carried out to determine the critical yield stress for various strain rates. From the calculated values, a master curve of the yield stress as a function of the strain rate is built at 300 K. It is found that the predicted results and experimental values are aligned on the same curve and can be described by a simple Cowper-Symonds relation. Furthermore, using the Williams, Landel and Ferry equation, a master curve is built to predict the yield stress at finite temperatures. By investigating additional deformation modes, two supplementary master curves are built at 300 K: one for the void nucleation and one for the shear yielding.

1. Introduction

In recent years, the continuous need for lightweight and high performance materials for automotive applications has brought manufacturers to use polymers for the design of light components. Polycarbonate (PC) is a typical example of a polymer material that offers unique properties such as high strength to weight ratio, high thermal resistance, optical transparency, etc. PC is frequently used as panoramic sunroof or car headlight covers however, for applications as car body elements, it is necessary to further reduce the thickness of the parts while maintaining their high toughness to withstand the impact of stones and other road debris that might hit the car body during driving.

For the development of automotive body panels based on PC, a profound knowledge of the mechanical properties of the material is mandatory. This information is commonly obtained from experiments involving various testing methods to characterize the materials properties. The corresponding material constitutive laws are then implemented into finite element programs for performing continuum model simulations of, e.g., fracture and deformations. Although this approach is well established in the industry, alternative approaches such as atomistic simulations have gained a growing interest due to recent advances in computational power and numerical algorithms. In this so-called bottom-up approach, valuable information from atomistic simulations is used for developing models capable of providing accurate predictions of the material's mechanical properties.

The yield stress is regarded as an important property to characterize the mechanical behavior of polymers and its dependence on strain rate and temperature is well known. This dependence is captured by master yield stress curves that are commonly used for predicting the yield stress at any strain rate and/or temperature [1].

The first works investigating the relationship between the yield stress and the strain rate in PC were carried out by Bauwens in the early to mid-1970s [2–4] where strain rates less than 1 s^{-1} were considered. The authors reported a linear dependence between the tensile yield stress and the logarithm of the strain rate [3].

In the past decade, strain rates up to $4.5\times10^{3}\,s^{-1}$ were achieved

* Corresponding author.
E-mail address: jan@ulab.iis.u-tokyo.ac.jp (J.-M. Albina).

https://doi.org/10.1016/j.polymer.2019.05.045
Received 27 February 2019; Received in revised form 13 May 2019; Accepted 18 May 2019
Available online 22 May 2019
0032-3861/

using dynamic techniques such as the split Hopkinson tension bar (SHTB). Various authors noticed that the yield stress values increased dramatically for higher strain rates [5–8]. A plot of the yield stress vs. strain rate would appear as bi-linear with a large gap in the data set between the quasi-static and SHTB data [8]. However, the experimental measurements at moderate strain rates ($0.5\,s^{-1}$–$32\,s^{-1}$) from Cao et al. [6] revealed a non-linear strain rate dependence of the yield stress.

Strain rates above $10^3\,s^{-1}$ can be currently achieved with computational approaches such as molecular dynamics (MD). All-atom (AA) and coarse-grained (CG) simulations are considered to be the most suitable approaches to investigate the mechanical properties of polymers at high-strain rates. In particular the CG method enables the simulation of more realistic and sophisticated models by extending the simulation time and length scale.

In the present work, a CG-potential was developed to estimate the yield stress of PC at high strain rates. The methodology and potential parameters are introduced in the first part of this paper. Applications of the CG potential for mechanical deformations in strained systems are presented in the second part where several master yield stress curves are built. Finally, a summary of results and discussion is provided in the last section.

2. Coarse-grained model

The strength of the CG method lies in its ability to simplify the complex chemical structure of a macromolecule by substituting its chemical groups for particles. As illustrated in Fig. 1, the molecular formula of PC consists of three groups of atoms: carbonate, phenylene and isopropylidene which are replaced in the CG model by the particle A, B, and C, respectively. A formula unit of PC containing 33 atoms is thus reduced to 4 particles.

2.1. Potential parametrizations

Numerous CG-based approaches for the modeling of PC have been developed over the last 20 years [9–13]. This work is an improvement of the CG-potential that was introduced in our previous work [14,15].

The total energy of our CG model is given by:

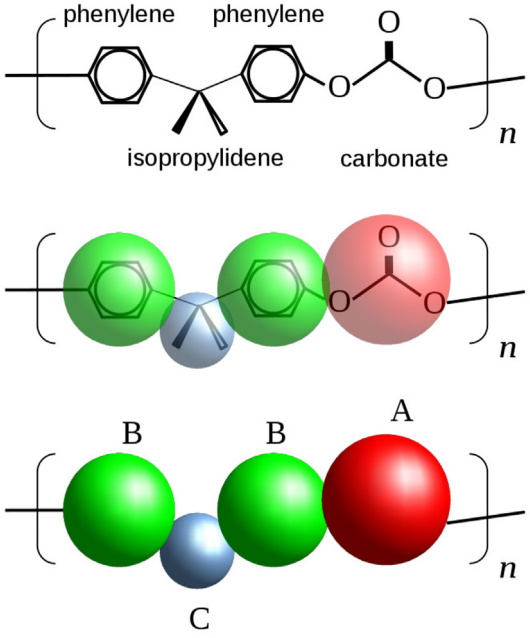

Fig. 1. Illustration of the CG mapping scheme for a PC monomer.

$$E_{\text{total}} = \underbrace{E_b + E_a}_{\text{bonding interaction}} + \underbrace{E_{nb}}_{\text{non-bond interaction}} \quad (1)$$

where the bonding interaction is given by the sum of the bond (E_b) and angle (E_a) terms. The non-bonding interaction is modeled by a pair potential.

The functional form of the terms used in Equation (1) are given by:

$$E_b = \sum_{n=2}^{4} K_n^b (r - r_0)^n \quad (2)$$

$$E_a = \sum_{n=2}^{4} K_n^a (\theta - \theta_0)^n \quad (3)$$

$$E_{nb} = \sum_{i<j} \Phi_{ij}(\bar{r}_{ij}) \quad (4)$$

with r, θ and $\bar{r}$ the bond length, bond angle and interparticle distance, respectively. The constants K_n^b, K_n^a, r_0 and θ_0 are potential parameters that are determined by AA molecular dynamics. In comparison to our previous CG model [14,15], no dihedral term is included in this model.

The dihedral angle (or torsion angle) is formed between two planes intersecting in 3-dimensional space. During deformation simulations, the PC chains can be strongly stretched if they do not have enough time to disentangle from each other. If such situation happens, the polymer chains are forced into a linear conformation and the dihedral angle cannot be evaluated. Consequently, a divergence instability occurs which can sometimes be recognized by a peak in the total potential energy and/or on the stress-strain curve. (An example of a stress-strain curve showing several peaks is shown on Fig. S5 in the supporting material). The consequence is particularly critical for the simulation of deformations where these instabilities are promoting void nucleation and, as a direct result the yield stress magnitude is underestimated.

This instability problem has been reported in the literature [16,17] and a possible solution is to change the potential functional form of the dihedral term. We found out that for PC the contribution of the dihedral term to the energy and forces is minimal and that it can be therefore safely omitted. We include in the supporting material as well a figure comparing several stress-strain curves with and without the dihedral term using our previous version of the CG model [14,15] (Fig. S6). Only strain rates higher than $10^9\ s^{-1}$ are presented. Indeed, for high strain rates, the simulation time is too short for a proper stretching of the polymer chains to occur and the instability is rarely observed.

2.2. CG potential parameters

2.2.1. Bonding interaction

Simulations were performed using the LAMMPS simulation package [18]. To parametrize the bonding interaction (Equation (1)) AA-MD simulations were performed on a 64-mer PC single chain using the COMPASS [19,20] all-atom force field. In order to ensure that the CG model can simulate properly the stress-strain behavior of PC under deformation, the fitting procedure includes a polymer chain under increasing external tension. A 64-mer chain is fixed at both ends and maintained at three separation distances (450 Å, 600 Å and 800 Å). The parameters are fitted by an iterative scheme and the fitting procedure is carried out simultaneously on the three chain lengths.

The CG potential parameters for the bonding interaction are given in Table 1.

2.2.2. Non-bond interaction

The pair potential functions for the non-bond interaction $\Phi_{ij}(\bar{r}_{ij})$ are optimized in order to reproduce typical material properties of PC, i.e., the radial distribution functions (RDFs) $g_{IJ}(\bar{r})$ for particle pairs (I, J = A, B,C), the mass density ρ, the bulk modulus B and the coefficient of thermal expansion (CTE) α. Especially to model the material's response to an external strain or stress, ρ, B and α need to be reproduced

Table 1
CG potential bonding parameters for PC.

	A-B	B–C
r_0 (Å)	3.70	3.40
K_2^b (kcal/mol Å^{-1})	10.0	80.0
K_3^b (kcal/mol Å^{-3})	0.00	300
K_4^b (kcal/mol Å^{-4})	1200	2000

	A-B-C	B-A-B	B–C–B
θ_0	180	180	76.0
K_2^a (kcal/mol rad^{-2})	−2.00	0.00	55.0
K_3^a (kcal/mol rad^{-3})	0.00	1.50	−1.00
K_4^a (kcal/mol rad^{-4})	20.0	1.00	1.00

with higher accuracy than the RDFs. The material properties (reference data) are obtained from AA-MD calculations.

Classically a 12-6 Lennard-Jones potential model is employed for the treatment of the non-bond interaction. However, softer types of potentials like the 9-6 Lennard-Jones or Morse potential have become favored models in the field of coarse-grained simulation [21,22]. We employed here the Morse potential function for the non-bond interaction. The functional form of the potential is:

$$\Phi_{IJ}(\bar{r}) = D_{0,IJ}\left[e^{-2\beta_{IJ}(\bar{r}-\bar{r}_{0,IJ})} - 2e^{-\beta_{IJ}(\bar{r}-\bar{r}_{0,IJ})}\right] \quad (5)$$

where $D_{0,IJ}$, β_{IJ} and $\bar{r}_{0,IJ}$ are potential parameters determined individually for each particle pair *I-J*. Hence, eighteen parameters in total have to be optimized.

The potential development procedure consists of three stages: (1) several AA-MD calculations are carried out to obtain basic properties of PC which are used as reference data for parametrization; (2) potential parameters are optimized to reproduce the RDFs as an initial guess; (3) the parameters are adjusted using universal scaling factors to fit the bulk properties ρ, *B* and *α*.

In the first stage, we performed AA-MD calculations to obtain the RDFs and the bulk properties mentioned above using a simulation cell with 128 PC chains consisting of 64 monomers each. The mass density was evaluated with a simulation cell equilibrated at 300 K and zero external stress. The bulk modulus *B* was evaluated from the change in volume under the hydrostatic stress $\sigma = -10$ MPa to + 10 MPa at 300 K. The CTE *α* was evaluated from the change in volume at $T = 200$ K to 400 K and zero external stress. The reference data of the RDF for each particle pair $\Phi_{IJ}^{\mathrm{ref}}(\bar{r})$ was obtained after converting the AA equilibrium structure (300 K, no external stress) into the CG representation.

During the second stage, we optimize the potential function Φ_{IJ} in a similar way as in the iterative Boltzmann inversion (IBI) scheme [23]. For each iteration step *n*, the RDFs $g_{IJ}^n(\bar{r})$ are evaluated with the *n*-th provisional potential function $\Phi_{IJ}^n(\bar{r})$ using a simulation cell with 128 PC chains consisting of 64 monomers each. The potential function at the $(n+1)$-th step $\Phi_{IJ}^{n+1}(\bar{r})$ is determined to fit $\Phi_{IJ}^n(\bar{r}) - k_{\mathrm{B}}T\ln(g_{IJ}^{\mathrm{ref}}(\bar{r})/g_{IJ}^n(\bar{r}))$; this procedure is a simple extension of the IBI scheme to any arbitrary analytic functions. Note that the potential function at this stage is still not optimized enough for reproducing the bulk properties.

In the third and final stage, we further modify the potential function obtained at the previous stage by scaling the potential parameters with universal scaling factors:

$$\begin{pmatrix} D_{0,IJ} \\ \beta_{IJ} \\ r_{0,IJ} \end{pmatrix} \mapsto \begin{pmatrix} c_1 \cdot D_{0,IJ} \\ c_2 \cdot \beta_{IJ} \\ c_3 \cdot r_{0,IJ} \end{pmatrix} \quad (6)$$

where c_1, c_2 and c_3 are the scaling factors that need to be optimized at this stage in order to reproduce the bulk properties ρ, *B* and *α*. The parameters c_1 and c_2 were changed in a stepwise manner and the parameter c_3 was independently adjusted for each pair of c_1 and c_2 to reproduce the mass density ρ at 300 K and $\sigma = 0$ MPa. A series of CG-MD calculations is performed to evaluate *B* and *α* with each scaling factor (c_1, c_2, c_3) under the same calculation conditions as the AA-MD calculations at the stage 1.

Table 2
CG potential non-bond parameters for PC. Each particle pair is represented by a Morse potential.

	A-A	A-B	A-C	B–B	B–C	C–C
D_0 [kcal/mol]	0.527	1.198	1.807	0.591	0.013	0.790
β [Å^{-1}]	1.157	0.755	0.764	0.812	1.452	1.060
$\bar{r}_0$ [Å]	4.984	5.520	5.547	5.838	6.465	5.788

The changes in RDF during the individual stages of the fitting procedure are shown in the supporting material (Fig. S4).

Table 2 lists the optimized potential parameters for the Morse potential with a cut-off radius $r_c = 12$ Å. The corresponding function profiles are shown in Fig. 3.

2.2.3. Fitting results

Probability density distributions obtained from AA-MD and CG-MD for the 450 Å chain are compared in Fig. 2. An examination of the curves shows a good agreement for the bond lengths. Bond angles are reproduced by the CG model as well except for the 'phenylene-carbonate-phenylene' (B-A-B) angle. A distribution with three peaks is observed in the AA simulation while only one peak is present in the CG model (see Fig. 2 b). The origin of the discrepancy is attributed to the inability of the mathematical model (Equation (3)) to reproduce multimodal distributions.

Table 3 lists the bulk properties obtained with the CG model and compares them to the AA-MD result and experimental values. Basic material properties of PC are reproduced with an excellent accuracy by the CG model. Especially, the error between CG-MD and AA-MD simulations for ρ and *α* is within 1%. Although a relatively large discrepancy is found for the bulk modulus *B*, the error is less than 20% and the CG-MD result lies in between those obtained by AA-MD and the experimental ones. The glass transition temperature T_g is determined from the change in slope of the specific volume as a function of the temperature curve. A theoretical value of 402 K is also in a good agreement with the experimental value of 420 K. Plots of the specific volume as a function of the temperature used for the determination of T_g are provided in the supporting material (Figs. S2 and S3).

With the good agreement of the coefficient of thermal expansion, we assume that the volume-pressure-temperature relationship is reasonably well reproduced in the temperature range from 100 K to 400 K. Temperatures above T_g were not investigated since the CG model might not capture all aspects of the material behavior at these temperatures.

3. Results and discussion

3.1. Mechanical deformations of PC

A simulation cell containing 4000 CG particles (equivalent to ca. 34,000 atoms) was used for deformation analyses. The system was initially annealed and equilibrated until the system becomes fully relaxed. The system was then cooled down to the target temperature for deformation analyses.

We investigate five types of deformations: (i) uniaxial tension with transverse strain constraints ($\varepsilon_{xx} = \varepsilon_{yy} = 0$ and $\varepsilon_{zz} = \dot{\varepsilon}t$), (ii) uniaxial tension without transverse strain constraints ($\sigma_{xx} = \sigma_{yy} = 0$, $\varepsilon_{zz} = \dot{\varepsilon}t$), (iii) uniform biaxial tension ($\sigma_{xx} = 0$, $\varepsilon_{yy} = \varepsilon_{zz} = \dot{\varepsilon}t$), (iv) uniform triaxial tension ($\varepsilon_{xx} = \varepsilon_{yy} = \varepsilon_{zz} = \dot{\varepsilon}t$), and (v) shear ($\sigma_{xx} = \sigma_{yy} = \sigma_{zz} = 0$, $\gamma_{xy} = \dot{\gamma}t$).

The CG-MD simulations were carried out using a Nosé-Hoover thermostat and barostat as implemented in LAMMPS. A time step of 2 fs was set for all CG-MD analyses.

The effect of molar mass, cell size and temperature on the

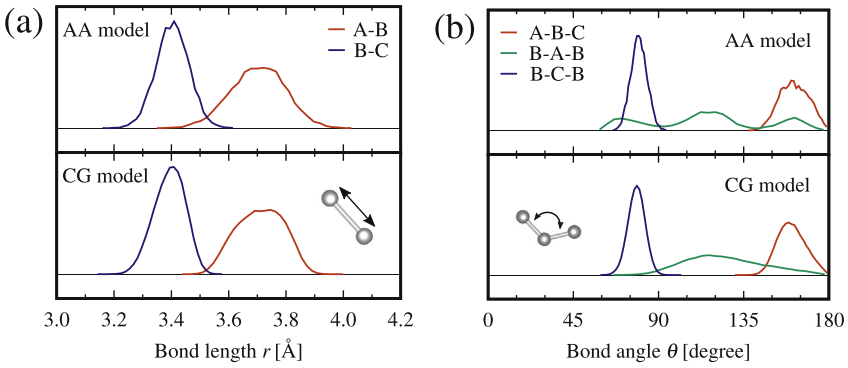

Fig. 2. Probability distributions of (a) bond lengths and (b) bond angles for a 64-mer single chain of PC fixed at 450 Å: comparison of the AA-MD model (upper panel) to the CG-MD model (lower panel).

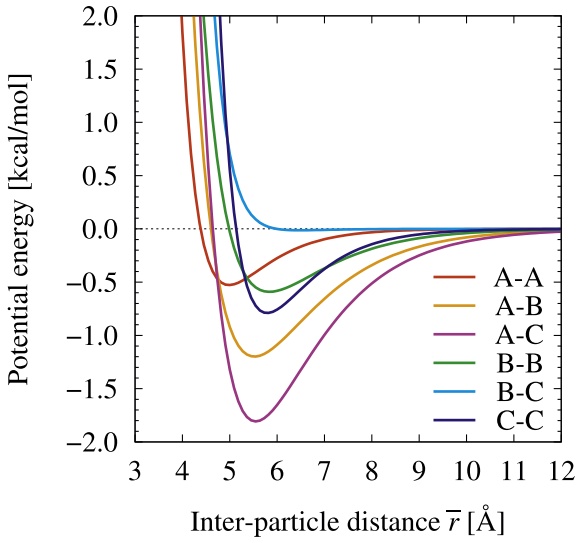

Fig. 3. Inter-particle potential (Equation (5)) for each particle pair in the CG model.

Table 3
Bulk properties of PC obtained by CG and AA models; mass density ρ, bulk modulus B, coefficient of thermal expansion α and glass transition temperature T_g.

	CG-MD	AA-MD	Experiment
ρ [g/cm^3]	1.19	1.19	1.19[c]
B [GPa]	2.90[a]	3.50[a]	2.36–2.64[c], 2.95–3.08[c]
α [10^{-6} K^{-1}]	63.1[b]	63.4[b]	65.0[d]
T_g [K]	402	–	420[e]

[a] Average value between $\sigma = -10$ MPa and + 10 MPa at 300 K.
[b] Average value between 200 K and 400 K with $\sigma = 0$ MPa.
[c] See Ref. [13] and references therein.
[d] Ref. [24].
[e] Ref. [25].

mechanical properties has already been discussed elsewhere in the literature [15].

Fig. 4a illustrates a typical stress-strain curve obtained from a uniaxial tensile test simulation with transverse strain constraints. The simulation cell contains 16 PC chains of each 64-mers ($\dot{\varepsilon} = 10^9$ s^{-1}, $T = 300$ K). Note that the curve shown in Fig. 4a is the result of a smoothing operation carried out with Bézier curve to minimize the noise in the raw data. The yield stress is determined from the maximum of the (smoothed) curve.

3.2. Master tensile yield stress curves

3.2.1. Master curve at 300 K

Fig. 4b shows the variation of the yield stress as a function of the strain rate at 300 K. The results from CG-MD are obtained for a range of high strain rates (10^6 s^{-1} to 10^{11} s^{-1}). Evaluation of the yield stress at lower timescales are computationally time consuming and only practical for small sizes of simulation cells that are not suitable for the study of deformations. For lower strain rates (10^{-3} s^{-1} to 10^3 s^{-1}), experimental measurements compiled from various sources [4–6,8] are added on the figure. Results from AA-MD simulations at high strain rates are added on the figure as well. The difference observed between CG-MD and AA-MD becomes larger as the strain rate increases. This effect is due to friction between atoms that is currently not reproduced in our CG model.

The plot shows an non-linear trend in the data across many orders of magnitude. A fit including the calculated data and experimental results is carried out using the Cowper-Symonds [26] equation:

$$\sigma_Y(\dot{\varepsilon}) = \sigma_0\left[1 + \left(\frac{\dot{\varepsilon}}{C}\right)^{1/\rho}\right] \tag{7}$$

where C and ρ are two material parameters and σ_0 is the static yield stress. From the fit presented in Fig. 4b, the parameters for PC at 300 K were determined as: $C = 347$ s^{-1}, $\rho = 11.64$ and $\sigma_0 = 49$ MPa. We compared the Cowper-Symonds equation to several alternative equations and obtained exactly the same fit with the more sophisticated co-operative equation [27,28] (see discussion in section 3.3).

It should be noted that the fit is highly sensitive to the dataset range used. For example, if only data from CG-MD are considered for the fit of the Cowper-Symonds equation, the parameters for PC at 300 K change to $C = 4.95$ s^{-1}, $\rho = 6.42 \times 10^{+10}$ and $\sigma_0 = 151$ MPa. Therefore, to ensure a good quality of the fit, a dataset covering a wide range of strain rate is highly desirable.

3.2.2. Multi-temperature master curve

By applying a lateral shift to the yield stress values obtained from CG-MD at different temperatures, it is possible to build a master curve which collapses all the data into a single line at a reference temperature. In Fig. 5, the horizontal shift is evaluated at 300 K by the Williams, Landel and Ferry method [29]. The relation between the shift factor a_T and temperature is expressed as:

$$\log a_T = \frac{C_1(T - T_S)}{C_2 + (T - T_S)} \tag{8}$$

where C_1 and C_2 are two material constants. T_S is a reference temperature specific to PC.

Using (−8.86, 101.6) [30] and 700 K for, respectively (C_1, C_2) and T_S, the data at different temperatures are shifted to the master curve at 300 K. The good correlation obtained between strain rate and temperature is suggesting that, by simply knowing the shift factor, prediction of the strain rate can be directly obtained at other finite

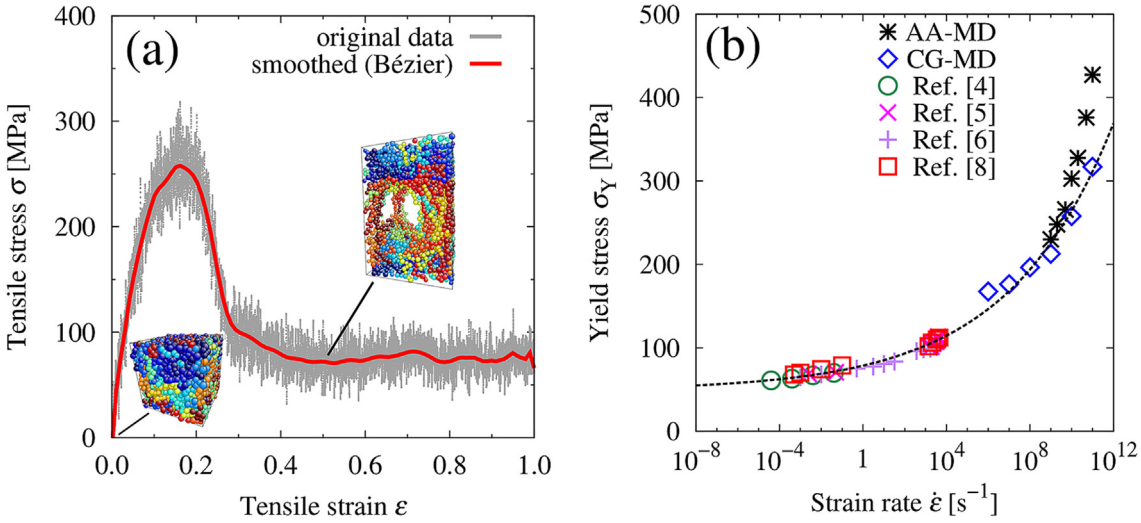

Fig. 4. (a) Representative stress-strain curve from a CG-MD simulation and a uniaxial tensile test with transverse strain constraints. (b) Yield stress as a function of the logarithm of the strain rate at 300 K for PC: CG-MD data are from this work, experimental results are compiled from Refs. [4–6,8]. The fit is carried out using the CG-MD data and experimental results.

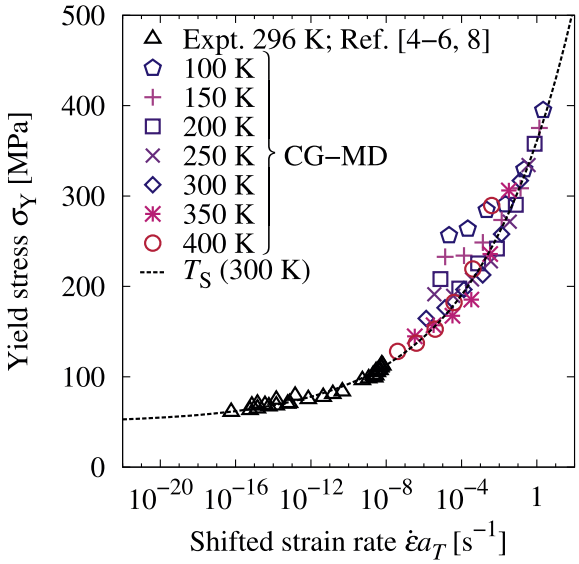

Fig. 5. Master curve for the yield stress as a function of the strain rate for PC under uniaxial tension. Data from CG-MD simulations at various temperatures are shifted onto a master curve at a reference temperature (T_S).

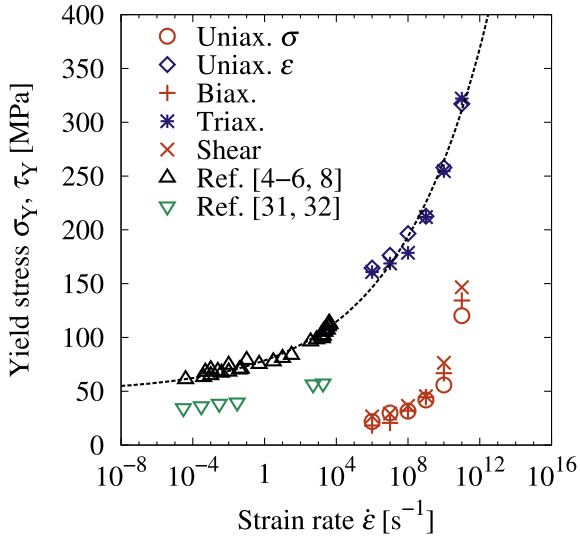

Fig. 6. Yield stress as a function of the strain rate for various deformations at a temperature of 300 K.

temperatures.

3.2.3. Multi-loading master curve at 300 K

In Fig. 6, additional deformation modes at 300 K are added on the original plot of the uniaxial tension. It is found that deformations can be grouped into two categories: the ones that leads to void nucleation and growth (constrained uniaxial tension and triaxial tension) and the ones where the structural integrity is maintained against distortion (unconstrained uniaxial tension, biaxial tension and shear). In the first category, the simulation cell undergoes a large volume expansion during deformation, which promotes the formation of voids. In the second category, the deformation modes are closely related to shear deformations. Indeed, the unconstrained uniaxial tension is geometrically equivalent to a shear deformation with a slight volume change if the cell symmetry axes are rotated by 45° with respect to the reference coordinate system. As for the biaxial tension, the deformation is equivalent to an unconstrained uniaxial compression and is therefore related to a shear deformation by the same rotation of 45°.

The values for the uniaxial and biaxial deformations reported on Fig. 6 are the resolved shear stresses of the corresponding deformations whose magnitudes are one half the yield stress values. Points marked as '×' are shear stresses obtained from CG-MD shear simulations. We added for comparison experimental shear stress values measured between 3×10^{-5} s^{-1} and 2×10^{3} s^{-1} in PC [31,32]. The experimental data show a trend towards higher values than the results obtained with CG-MD. The underestimation of the yield stress for the shear deformations is basically attributed to the oversimplified description of the molecular structure in the CG model. The shear deformation occurring under unconstrained uniaxial/biaxial stress conditions is caused by the sliding of molecular chains on each other. The behavior of molecules in such situation is closely related to the detailed atomistic structure of the molecular chains, which is not taken into account in the CG model. In other words, the surface of the CG particles is too smooth to experience an inter-molecular friction or viscous retardation, thus particles can slide (or move) more easily than in the all-atom structures. On the other hand, when the volume expansion under stress plays the most important role and when void nucleation is expected as in the case of triaxial stress conditions, the yield stress (and bulk modulus) can be

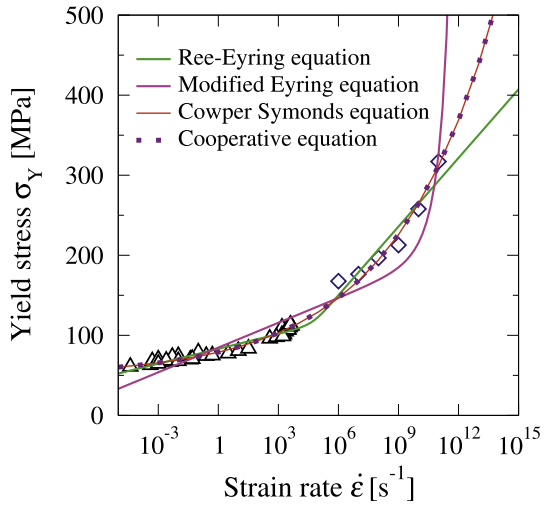

Fig. 7. Fit comparison for the yield stress as a function of the strain rate under uniaxial tension. Open symbols are experimental measurements [4–6,8]. Solid symbols are predicted results from CG-MD simulations.

Table 4
Comparison of the parameters for the cooperative equation (coop.) and the Cowper-Symonds (CS) equation.

Parameter	This work	Ref. [34]
coop./CS	coop./CS	coop./–
σ_i / σ_0	49.2/49.2	57.2/–
V/–	6.7×10^{-25} /–	1×10^{-28} /–
$\dot{\varepsilon}^*$ /–	$2.9 \times 10^{+30}$ /–	3465/–
n/ρ	11.64/11.64	7.82/–
–/C	–/347.6	–/–

well reproduced by simply adjusting the non-bond term.

Note that the above-mentioned problem about underestimation of stress (or elastic modulus) is the case not only in the present model but also in general CG models with simple descriptions of the non-bond interaction. Thus, for a quantitative evaluation of the stress or elastic modulus, a more complex formulation of the non-bond interaction is inevitable; e.g., several additional terms may be introduced to describe viscous and/or frictional forces exerted on the molecular chains. Alternative approaches involve the use of dissipative particle dynamics or Lowe-Andersen dynamics [33]. We plan to address this issue in a future development of the CG model.

3.3. Comparison of constitutive equations for the yield stress in PC

The Cowper-Symonds equation [26] is used for fitting both sets of experimental and simulation data. Three alternative equations are compared to the Cowper-Symonds model: the Ree-Eyring, the modified Eyring and the cooperative equations. For a listing of these constitutive equations, the reader is referred to other publications on the topic (e.g., Ref. [34]).

The Cowper-Symonds equation is chosen here due to its simplicity and general ease of implementation in finite element softwares.

As seen in Fig. 7, while the Cowper-Symonds equation is remarkably similar to the cooperative equation, the Ree-Eyring and modified Eyring models are not able to fit the data properly within the strain rate range.

The cooperative equation [27,28] has the following form:

$$\sigma_Y = \sigma_i + \frac{2k_B T}{V}\sinh^{-1}\left(\frac{\dot{\varepsilon}}{\dot{\varepsilon}^*}\right)^{\frac{1}{n}} \quad (9)$$

where σ_i, V, $\dot{\varepsilon}^*$ and n are the internal stress, the activation volume, the characteristic strain rate and a material parameter, respectively.

Table 4 compares the parameters obtained from a fit to the Cowper-Symonds and cooperative equations. It is striking to note that the internal stress and exponential parameters of both equations are identical, thus indicating the validity of the Cowper-Symonds equation for the construction of master yield stress curves in PC. The activation volume V and characteristic strain rate $\dot{\varepsilon}^*$ in the cooperative equation have been found to be highly sensitive to the initial guess in the fitting procedure and, as a consequence, it is very difficult to obtain consistent values for these two parameters. The discrepancy with the parameters published in Ref. [34] is attributed to the different dataset used for fitting. In their work, the authors used exclusively the experimental data of Cao et al. [6].

4. Summary and conclusion

A CG particle model for the simulation of deformation processes in PC was developed. Various tensile deformations were applied on a simulation containing 4000 CG particles (equivalent to ca. 34,000 atoms). Under uniaxial tension, the yield stress is reported for several high-strain rates and a fit using both experimental results and simulation values is carried out with the Cowper-Symonds [26] constitutive equation. Despite being a very general model, the Cowper-Symonds model produces the same result as the cooperative [27,28] model for a strain rate range between 10^{-6} s^{-1} to 10^{11} s^{-1}. The critical stress as a function of the logarithm of the strain rate follows an non-linear trend and the static yield stress at 300 K is found to be 49 MPa.

The Williams, Landel and Ferry equation [29] is used for constructing a master curve that includes yield stresses at different temperatures. The 300 K master curve is built from a shift factor a_T which depends on two constants (C_1, C_2) and a reference temperature (T_S) whose values are reported in the results section.

Finally, different deformation modes were investigated. The deformation modes can be classified into two main categories according to their mechanical response to external loading: (a) deformations leading to void nucleation and growth and (b) shear deformations. The triaxial tension and constrained uniaxial tension belong to the first category and are found lying on the same line (see Fig. 6). The unconstrained uniaxial tension, biaxial tension and shear belong to the second category and their shear stress values fall on a clear and unique trend line (Fig. 6). However, compared to experimental measurements of the shear stress in PC, the shear stress obtained from CG-MD simulations are found to be strongly underestimated. This is due to the absence of friction in our CG potential and this issue shall be addressed in a future improvement of the model.

Acknowledgments

This research was supported by Council for Science, Technology and Innovation (CSTI), Cabinet Office, Japan, through the ImPACT Program (Funding agency: JST, Japan Science and Technology Agency). The authors gratefully acknowledge Dr. M. Mrovec (ICAMS, Ruhr-Universität Bochum) for providing helpful comments on the manuscript.

Appendix A. Supplementary data

Supplementary data to this article can be found online at https://doi.org/10.1016/j.polymer.2019.05.045.

References

[1] C. Bauwens-Crowet, J. Bauwens, G. Homes, Tensile yield-stress behavior of glassy polymers, J. Polym. Sci. A-2 Polym. Phys. 7 (4) (1969) 735–742.
[2] J. Bauwens, C. Bauwens-Crowet, G. Homes, Tensile yield-stress behavior of poly (vinyl chloride) and polycarbonate in the glass transition region, J. Polym. Sci. A-2 Polym. Phys. 7 (10) (1969) 1745–1754.
[3] C. Bauwens-Crowet, J.-C. Bauwens, G. Homes, The temperature dependence of

yield of polycarbonate in uniaxial compression and tensile tests, J. Mater. Sci. 7 (2) (1972) 176–183.
[4] C. Bauwens-Crowet, J.-M. Ots, J.-C. Bauwens, The strain-rate and temperature dependence of yield of polycarbonate in tension, tensile creep and impact tests, J. Mater. Sci. 9 (7) (1974) 1197–1201.
[5] S. Sarva, M. Boyce, Mechanics of polycarbonate during high-rate tension, J. Mech. Mater. Struct. 2 (10) (2007) 1853–1880.
[6] K. Cao, X. Ma, B. Zhang, Y. Wang, Y. Wang, Tensile behavior of polycarbonate over a wide range of strain rates, Mater. Sci. Eng. A 527 (16–17) (2010) 4056–4061.
[7] J.L. Jordan, C. Siviour, B. Woodworth, High strain rate tensile and compressive effects in glassy polymers, EPJ Web of Conferences, vol. 26, EDP Sciences, 201201001.
[8] Y. Xu, T. Gao, J. Wang, W. Zhang, Experimentation and modeling of the tension behavior of polycarbonate at high strain rates, Polymers 8 (3) (2016) 63.
[9] W. Tschöp, K. Kremer, J. Batoulis, T. Bürger, O. Hahn, Simulation of polymer melts. I. coarse-graining procedure for polycarbonates, Acta Polym. 49 (2–3) (1998) 61–74.
[10] C.F. Abrams, K. Kremer, Combined coarse-grained and atomistic simulation of liquid bisphenol A-polycarbonate: liquid packing and intramolecular structure, Macromolecules 36 (1) (2003) 260–267.
[11] B. Hess, S. León, N. Van Der Vegt, K. Kremer, Long time atomistic polymer trajectories from coarse grained simulations: bisphenol-A polycarbonate, Soft Matter 2 (5) (2006) 409–414.
[12] C.K. Choudhury, P. Carbone, S. Roy, Scalability of coarse-grained potentials generated from iterative Boltzmann inversion for polymers: case study on polycarbonates, Macromol. Theory Simul. 25 (3) (2016) 274–286.
[13] K. Palczynski, A. Wilke, M. Paeschke, J. Dzubiella, Molecular modeling of polycarbonate materials: glass transition and mechanical properties, Physical Review Materials 1 (4) (2017) 043804.
[14] A. Kubo, Y. Umeno, Coarse-grained molecular dynamics simulation of fracture problems in polycarbonate, Solid State Phenomena, vol. 258, Trans Tech Publ, 2017, pp. 73–76.
[15] A. Kubo, Y. Umeno, Atomistic-level simulation of deformation in polycarbonate, Key Engineering Materials, vol. 725, Trans Tech Publ, 2017, pp. 445–450.
[16] A. Blondel, M. Karplus, New formulation for derivatives of torsion angles and improper torsion angles in molecular mechanics: elimination of singularities, J. Comput. Chem. 17 (9) (1996) 1132–1141.
[17] M.P. Howard, A. Statt, A.Z. Panagiotopoulos, Note: smooth torsional potentials for degenerate dihedral angles, J. Chem. Phys. 146 (22) (2017) 226101.
[18] S. Plimpton, Fast parallel algorithms for short-range molecular dynamics, J. Comput. Phys. 117 (1) (1995) 1–19.
[19] H. Sun, S.J. Mumby, J.R. Maple, A.T. Hagler, An ab initio CFF93 all-atom force field for polycarbonates, J. Am. Chem. Soc. 116 (7) (1994) 2978–2987.
[20] H. Sun, COMPASS: an ab initio force-field optimized for condensed-phase applications overview with details on alkane and benzene compounds, J. Phys. Chem. B 102 (38) (1998) 7338–7364.
[21] C. Peter, L. Delle Site, K. Kremer, Classical simulations from the atomistic to the mesoscale and back: coarse graining an azobenzene liquid crystal, Soft Matter 4 (4) (2008) 859–869.
[22] A. Chakrabarty, T. Cagin, Coarse grain modeling of polyimide copolymers, Polymer 51 (12) (2010) 2786–2794.
[23] D. Reith, M. Pütz, F. Müller-Plathe, Deriving effective mesoscale potentials from atomistic simulations, J. Comput. Chem. 24 (13) (2003) 1624–1636.
[24] G. Abts, T. Eckel, R. Wehrmann, Polycarbonates, Ullmann's Encyclopedia of Industrial Chemistry, Wiley-VCH Verlag GmbH & Co. KGaA, 2014.
[25] D.J. Plazek, K.L. Ngai, The glass temperature, Physical Properties of Polymers Handbook, Springer, 2007, pp. 187–215.
[26] G.R. Cowper, P.S. Symonds, Strain-hardening and Strain-Rate Effects in the Impact Loading of Cantilever Beams, Tech. Rep. Brown Univ Providence Ri, 1957.
[27] J. Richeton, S. Ahzi, L. Daridon, Y. Rémond, A formulation of the cooperative model for the yield stress of amorphous polymers for a wide range of strain rates and temperatures, Polymer 46 (16) (2005) 6035–6043.
[28] J. Richeton, S. Ahzi, K. Vecchio, F. Jiang, R. Adharapurapu, Influence of temperature and strain rate on the mechanical behavior of three amorphous polymers: characterization and modeling of the compressive yield stress, Int. J. Solids Struct. 43 (7–8) (2006) 2318–2335.
[29] J.D. Ferry, Viscoelastic Properties of Polymers, John Wiley & Sons, 1980.
[30] K. Tsunoda, J. Busfield, C. Davies, A. Thomas, Effect of materials variables on the tear behaviour of a non-crystallising elastomer, J. Mater. Sci. 35 (20) (2000) 5187–5198.
[31] C. G'sell, A. Gopez, Plastic banding in glassy polycarbonate under plane simple shear, J. Mater. Sci. 20 (10) (1985) 3462–3478.
[32] N.A. Fleck, W. Stronge, J. Liu, High strain-rate shear response of polycarbonate and polymethyl methacrylate, Proceedings of the Royal Society of London. A. Mathematical and Physical Sciences 429 (1877) (1990) 459–479.
[33] H.-J. Qian, C.C. Liew, F. Müller-Plathe, Effective control of the transport coefficients of a coarse-grained liquid and polymer models using the dissipative particle dynamics and Lowe–Andersen equations of motion, Phys. Chem. Chem. Phys. 11 (12) (2009) 1962–1969.
[34] A.A. Al-Juaid, R. Othman, Modeling of the strain rate dependency of polycarbonate's yield stress: evaluation of four constitutive equations, J. Eng. (2016) 6315421.